4D-PreNet: A Unified Preprocessing Framework for 4D-STEM Data Analysis

Mingyu Liu[1], Zian Mao[1,2*], Zhu Liu[1,3], Haoran Zhang[1,2], Jintao Guo[1], Xiaoya He[1,2], Xi Huang[1], Shufen Chu[1], Chun Cheng[1], Jun Ding[4], Yujun Xie[1*]

[1]Global Institute Of future Technology, Shanghai Jiao Tong University, No. 800 Dongchuan Road, Minhang District, Shanghai, 200240, China.

[2]University of Michigan–Shanghai Jiao Tong University. Joint Institute, Minhang District, Shanghai, 200240, China.

[3]School of Chemistry and Chemical Engineering, Shanghai Jiao Tong University, Minhang District, Shanghai, 200240, China.

[4]Center for Alloy Innovation and Design, State Key Laboratory for Mechanical Behavior of Materials, Xi'an Jiaotong University, Xi'an 710049, PR China.

Abstract

Automated experimentation with real time data analysis in scanning transmission electron microscopy (STEM) often require end-to-end framework. The four-dimensional scanning transmission electron microscopy (4D-STEM) with high-throughput data acquisition has been constrained by the critical bottleneck results from data preprocessing. Pervasive noise, beam center drift, and elliptical distortions during high-throughput acquisition inevitably corrupt diffraction patterns, systematically biasing quantitative measurements. Yet, conventional correction algorithms are often material-specific and fail to provide a robust, generalizable solution. In this work, we present 4D-PreNet, an end-to-end deep-learning pipeline that integrates attention-enhanced U-Net and ResNet architectures to simultaneously perform denoising, center correction, and elliptical distortion calibration. The network is trained on large, simulated datasets encompassing a wide range of noise levels, drift magnitudes, and distortion types, enabling it to generalize effectively to experimental data acquired under varying conditions. Quantitative evaluations demonstrate that our pipeline reduces mean squared error by up to 50% during denoising and achieves sub-pixel center localization in the center detection task, with average errors below 0.04 pixels. The outputs are bench-marked against traditional algorithms, highlighting improvements in both noise suppression and restoration of diffraction patterns, thereby facilitating high-throughput, reliable 4D-STEM real-time analysis for automated characterization.

Keywords Preprocessing Framework, Convolutional Neural Networks, Noise Reduction, Center Shift Calibration, Elliptical Distortion Calibration

Introduction

Automated experimentation with real-time data analysis in scanning transmission electron microscopy (STEM) is an emerging tool for unlocking the atomic-scale

mechanisms that govern material properties[1, 2]. A key requirement for this automation is moving beyond the labor-intensive feature engineering of traditional machine learning[2]. End-to-end learning models provide the solution by streamlining this process, training a single, unified neural network to perform the complete task from raw input to final output. However, this approach generally requires vast amounts of labeled data to learn effectively and avoid overfitting, a constraint that makes it infeasible for many conventional STEM applications.

4D-STEM has emerged as an ideal platform for such automated experiments due to its inherently high-throughput data acquisition. In conventional methods, analysis of the rich datasets from 4D-STEM enables high-resolution mapping of strain fields, lattice orientations, and crystal defects by recording a 2D diffraction pattern at every 2D probe position[3]. However, the transformative potential of 4D-STEM is fundamentally undermined by artifacts inherent to the acquisition process. Low-dose imaging introduces pervasive random noise[4], while optical misalignment and sample drift cause shifts in the diffraction pattern center[5, 6, 7]. Furthermore, lens aberrations and detector imperfections induce elliptical distortions, warping the intrinsic symmetries of the diffraction space[8]. These artifacts inevitably require careful calibration for any subsequent quantitative analysis, creating a significant bottleneck for a truly end-to-end workflow.

More importantly, these artifacts are not mere imperfections but a critical barrier to quantitative analysis. In principle, even a sub-pixel error in locating the beam center can propagate into significant, non-physical variations in measured strain fields, while distortions can alter symmetry relationships used for phase identification. In the study by Zeltmann, optimizing the precise localization of diffraction spots improved the precision of subsequent strain measurements in Si samples by 80%[4]. Elliptical distortion can also lead to significant errors in the measurement of tetragonal distortion (T); Nicolopoulos et al. demonstrated that an uncorrected 5% elliptical distortion introduced T errors comparable to the actual distortion magnitude, whereas correction reduced the errors to below 1%[9]. Similarly, for noise, low-dose imaging required for beam-sensitive materials results in strong noise that obscures diffraction details, severely limiting the accuracy of strain and orientation measurements. Therefore, effective preprocessing methods addressing these three types of artifacts—noise, beam center drift, and elliptical distortion are essential for achieving high-precision quantitative analysis.

To mitigate these issues, a suite of correction algorithms has consistently been developed. Classical methods, such as singular value decomposition (SVD) for denoising[5] and circular Hough transforms for center finding[10], have been integrated into powerful community frameworks like py4DSTEM[11]. More recently, deep learning has been applied to advancing scientific research in electron microscopy and isolated tasks[12, 13, 14, 15, 16, 17, 18, 19, 20, 21, 22], including unsupervised denoising[23] and CNN-based or transformer-based center localization[24, 25]. Yet, these approaches remain piecemeal solutions. Conventional methods require tedious, manual parameter tuning for each dataset, while existing deep learning models typically address only a single artifact at a time, failing to account for the coupled nature of these distortions.

Consequently, a robust, general-purpose, and fully automated preprocessing workflow has remained out of reach.

The absence of an integrated solution can be attributed to several key challenges. First, jointly correcting multiple distinct artifacts—such as noise, beam drift, and elliptical distortion—within a single network architecture is inherently difficult due to potential task interference and architectural complexity. Second, the absence of large-scale annotated datasets, especially those containing ground truth for latent distortion parameters, limits both supervised learning and objective benchmarking. Third, the interdisciplinary nature of the problem—spanning materials science, electron microscopy, and deep learning—has posed barriers to progress. Consequently, no unified model currently exists that can robustly preprocess 4D-STEM data across diverse material systems.

Here, we present for the first time a unified, end-to-end deep learning framework for 4D-STEM preprocessing, termed 4D-PreNet, which concurrently performs diffraction denoising, beam center correction, and elliptical distortion rectification. By integrating three dedicated yet interconnected convolutional neural network (CNN) modules into a single pipeline, 4D-PreNet learns to disentangle and correct convoluted artifacts directly from the experimental data. Applicable to both crystal and amorphous materials, the framework dramatically improves the accuracy, robustness, and throughput of 4D-STEM analysis. We validate 4D-PreNet on both simulated and experimental datasets, demonstrating its ability to restore diffraction patterns to near-ideal conditions by "one-click", which pave the way for reliable, high-throughput, and truly quantitative atomic-scale materials characterization.

Method

Task-specific convolutional neural network (CNN) architectures were employed to address three fundamental preprocessing challenges in 4D scanning transmission electron microscopy, namely denoising, beam center calibration and elliptical distortion correction. For denoising and center localization, which both involve pixel-wise image reconstruction and spatial localization, we adopted the U-Net architecture with an encoder–decoder structure and skip connections. U-Net is widely recognized for its ability to preserve fine structural details while enabling accurate localization in dense prediction tasks[26].In contrast, elliptical distortion correction requires a global geometric regression strategy; therefore, we utilized a modified ResNet architecture, which provides strong feature extraction capabilities and robustness in modeling spatially global patterns27. All models were implemented using the PyTorch deep learning framework.

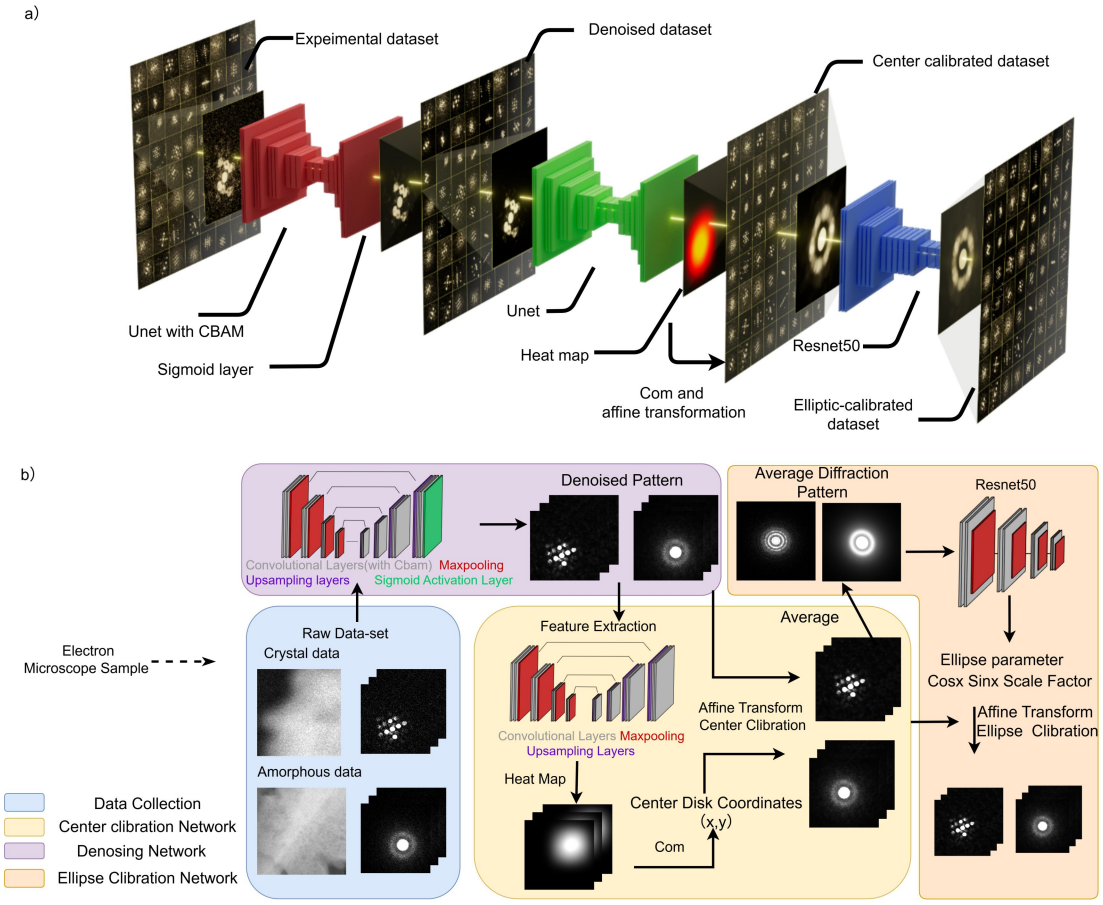

Figure 1 Three-stage deep learning framework (4D-PreNet) for fully automated 4D-STEM preprocessing a). Overview of the end-to-end three-stage deep-learning pipeline for 4D-STEM data preprocessing. The network consists of a U-Net with CBAM for denoising, a second U-Net for center localization and affine transformation, and a ResNet50-based regression model for predicting elliptical distortion parameters. This pipeline directly operates on raw 4D data cubes and produces fully corrected datasets with improved circular symmetry. b). Detailed workflow illustrating denoising, center detection, and ellipse calibration networks with intermediate outputs. Raw 4D-STEM data from both crystal and amorphous regions are first denoised to suppress Poisson and Gaussian noise. A heatmap regression network estimates center positions, which are then aligned through affine calibration. The averaged diffraction pattern is used to extract ellipticity parameters, which are regressed by ResNet50 to guide elliptical correction. The entire pipeline is trained to generalize across diverse structures and enables high-throughput, fully automated processing.

For the denoising module, we incorporated a Convolutional Block Attention Module (CBAM)[28] into the U-Net backbone to enhance spatial feature representation. A sigmoid activation was used in the final layer to ensure non-negative outputs, consistent with the physical nature of diffraction intensities[29]. The network was trained to suppress both Poisson and Gaussian noise, recovering high-frequency structural features critical for downstream analysis[30, 31]. Subpixel-accurate coordinates

were extracted using a weighted center-of-mass calculation based on the predicted heatmap. Each diffraction frame was then realigned using an affine transformation centered at the predicted coordinates. To maintain inference efficiency and avoid overfitting, we excluded the CBAM module in this task, as the required global context could be effectively captured without attention mechanisms.

To address elliptical distortion in diffraction patterns, we implemented a regression network based on ResNet-50 to predict three geometric parameters that define an affine correction: the cosine and sine of the major axis angle relative to the x-axis, and the aspect ratio between the principal axes. Instead of directly regressing the angular parameter, which introduces discontinuities at periodic boundaries, we adopted the continuous and differentiable formulation of the orientation using its sine and cosine components. This approach has been widely applied in pose estimation and orientation regression tasks, as it improves training stability and robustness to symmetry–induced ambiguities

The beam center calibration module also employed a U-Net architecture to predict a 2D heatmap representing the probability distribution of the beam center location[32, 33]. Subpixel-accurate coordinates were extracted using a weighted center-of-mass calculation based on the predicted heatmap. Each diffraction frame was then realigned using an affine transformation centered at the predicted coordinates. To maintain inference efficiency and avoid overfitting, we excluded the CBAM module in this task, as the required global context could be effectively captured without attention mechanisms.

To address elliptical distortion in diffraction patterns, we implemented a regression network based on ResNet-50 to predict three geometric parameters that define an affine correction: the cosine and sine of the major axis angle relative to the x-axis, and the aspect ratio between the principal axes. Instead of directly regressing the angular parameter, which introduces discontinuities at periodic boundaries, we adopted the continuous and differentiable formulation of the orientation using its sine and cosine components. This approach has been widely applied in pose estimation and orientation regression tasks, as it improves training stability and robustness to symmetry–induced ambiguities[34, 35, 36]. The residual network architecture enables the model to effectively learn global geometric deformations, allowing for accurate restoration of circular symmetry even in the presence of significant noise or partially missing diffraction rings.

Training Dataset Creation

We generated a large-scale simulation dataset for 4D-STEM analysis. In total, 1,024 structures—comprising both crystal and amorphous materials—were randomly selected from publicly available CIF databases such as the Materials Project[37].

Diffraction patterns were simulated using the abTEM library, which implements the multi-slice algorithm for realistic STEM simulations. Two distinct datasets were prepared to support different training objectives, reflecting the diversity and complexity encountered in experimental 4D-STEM data[4, 38].

The first dataset was designed for training denoising and center detection networks.

To create a diverse dataset, each CIF was rotated to sample a wide range of crystallographic orientations, and experimental parameters such as convergence semi-angle were randomly varied for each pattern. Synthetic distortions were applied by introducing random x- and y-shifts to simulate beam center displacement, along with random rotations and scaling to generate elliptical distortions. For amorphous patterns, similar procedures were followed to enhance dataset diversity. The augmented diffraction patterns and their corresponding center coordinates were saved as training data. To better control the noise characteristics, noise was added only at the network input stage, using the noiseless images as labels for the denoising task, and the accurate center coordinates as labels for the center detection task.

The second dataset was created for training the elliptical distortion calibration network. To simulate realistic experimental scenarios involving the stacking of multiple diffraction patterns, each CIF was first simulated with a fixed set of experimental parameters, then rotated to generate diffraction patterns at different crystallographic orientations. For each CIF, two sets of experimental parameters were used, with each set producing 128 patterns. These 128 patterns were further augmented by 30 random rotations to increase orientation diversity, yielding 3840 patterns per CIF per parameter set. From these, 3000 patterns were randomly selected and combined with mixed noise and random affine transformations (rotations and scaling) to simulate elliptical distortions. For each CIF and experimental parameter combination, 100 composite diffraction patterns with associated distortion parameters were generated. Across all 1,024 CIF files, this yielded approximately 102,400 simulated diffraction patterns for training the elliptical distortion calibration model. Each averaged diffraction pattern is associated with a set of ellipse parameters—the cosine and sine of the major axis angle, and a scale factor—which serve as the ground truth labels for the simulated dataset. The number of diffraction patterns extracted per CIF can be flexibly adjusted according to available computational resources. In addition, synthetic noise can be introduced during training to improve the robustness of the model.

All datasets were partitioned into training, validation, and testing subsets. Model optimization was performed using the Adam optimizer, incorporating learning rate scheduling and early stopping based on the validation loss to prevent overfitting and accelerate convergence[32, 39]. Detailed descriptions of the training protocols, and hyperparameter configurations are provided in the Supplementary Information.

Results and discussion

The performance of the proposed preprocessing system was comprehensively evaluated on both simulated and experimental 4D-STEM datasets. To ensure generalizability, all evaluation data were generated independently from the training set, using randomized crystal orientations and simulation parameters. The evaluation focused on three key tasks: denoising, center calibration, and elliptical distortion calibration—across both amorphous and crystal samples.

Denoising Network

It is evident that the denoised outputs closely match the clean ground truth, effectively preserving high-frequency diffraction features while substantially reducing background noise. The residual maps in the rightmost column further corroborate the accuracy of the denoising process, revealing both uniformly distributed Gaussian noise and signal-dependent Poisson noise, which confirms the network's capability to suppress multiple noise types.

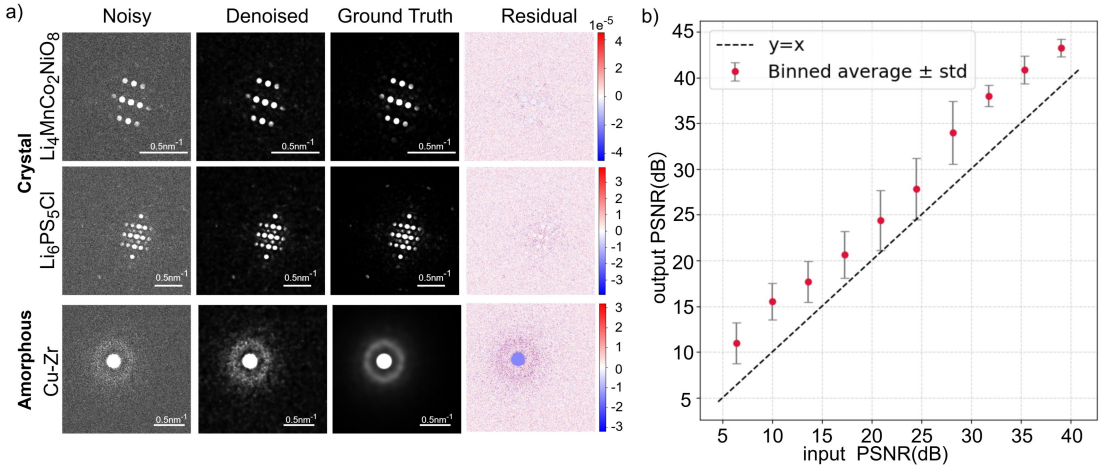

Figure 2: **Evaluation of denoising performance across noise levels in 4D-STEM diffraction patterns** a) Visual comparison of denoising performance across four representative diffraction patterns. b) Output PSNR from 4D-PreNet denoised data with input PSNR from noisy data calculated under different noise levels

The proposed preprocessing framework was comprehensively validated on both simulated and experimental 4D-STEM datasets, encompassing both crystal and amorphous samples. As shown in Figure 2a), the denoised patterns exhibit sharply defined diffraction disks with significantly reduced noise levels compared to the noisy inputs. Notably, both the crystal (Li_6PS_5Cl, $Li_4MnCo_2NiO_8$) and amorphous (Cu–Zr) patterns demonstrate similar denoising trends, highlighting the model's robust generalization across different structural types. As illustrated in Figure 2b), the denoising network consistently improves the PSNR across varying noise levels, even when applied to test data not encountered during training, highlighting its strong generalization performance and stability.

Collectively, these results demonstrate that the proposed denoising approach not only enhances the signal-to-noise ratio but also faithfully preserves critical diffraction details, which is essential for accurate downstream analyses such as center calibration and elliptical distortion calibration.

Quantitative metrics are summarized in Supplementary Table. S1, which compares the MSE and PSNR before and after denoising. The results show consistent improvements across all tested samples. In both amorphous and crystal cases, the denoising network significantly reduces the Mean Squared Error (MSE) and increases the Peak Signal-to-Noise Ratio (PSNR). On average, MSE is reduced by more than 50%, while PSNR improves by approximately 5–10 dB These results demonstrate the robustness of the model in handling both highly disordered amorphous structures and

periodic crystal patterns

Center Detection and Calibration

In the beam center calibration task, we propose a U-Net-based deep neural network that integrates heatmap regression with the center of mass (CoM) calculation to achieve sub-pixel accuracy in beam localization. This method is systematically compared against three mainstream center localization approaches: the conventional CoM method, the Friedel symmetry method, and the existing DPC segmentation network[24]. Evaluated on a test set comprising 4,096 simulated diffraction patterns, our method demonstrates superior localization accuracy. As illustrated in Figure3a), the model successfully corrects both systematic and stochastic beam shifts, achieving precise alignment of the beam center. Visual comparisons of pre- and post-calibration diffraction patterns from both crystal and amorphous samples further confirm the method's robustness and generalizability across structural types.

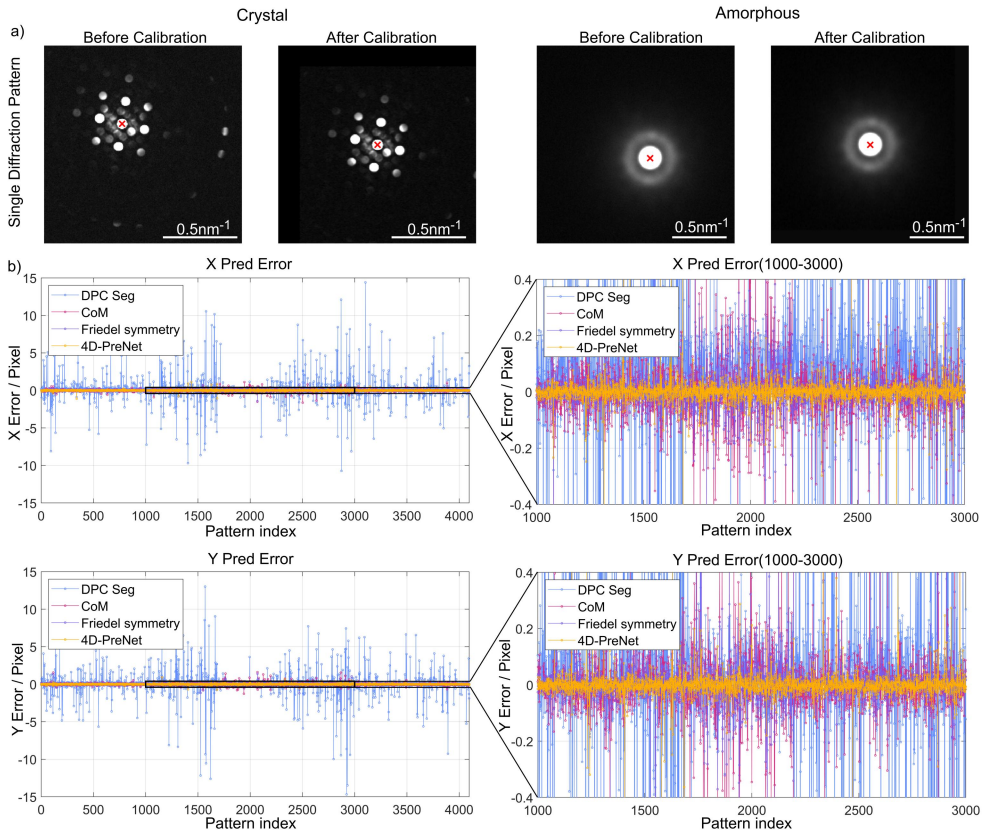

Figure 3: Comparison results of four center positioning methods on crystal and amorphous simulation data. (a) crystal calibration image; (b) amorphous calibration image (c) Prediction error distribution map in X-axis and Y-axis directions;

Figure 3b) shows the distribution of prediction errors along the X and Y directions. Compared with the three baseline methods—including the segmentation model used in DPC—the proposed 4D-PreNet model exhibits notably lower mean and variance in prediction errors. Quantitative results summarized in Supplementary Table. S2 support this observation: our model achieves the lowest mean absolute errors in radial

(MAE-R = 0.034), X-direction (MAE-X = 0.022), and Y-direction (MAE-Y = 0.021) localization. Compared to the second-best method (Friedel symmetry), the average error is reduced by more than 60%, while the reduction exceeds 90% relative to the DPC segmentation network.

Conventional center correction strategies typically rely on estimating a global average beam position from a set of diffraction patterns, aligning all images to this reference. While effective in small-scale or static datasets, such approaches are inherently unsuitable for real-time or high-throughput applications, where spatial consistency and frame-by-frame reliability are critical. In this study, we adopt a per-pattern calibration strategy that directly aligns each diffraction pattern to the geometric center of the image frame (e.g., (127.5, 127.5) for 256×256-pixel image), without relying on assumptions about the global beam position distribution.

This design offers key advantages for automated electron microscopy pipelines. By standardizing the coordinate system at the individual frame level, it ensures seamless compatibility with downstream processes such as pattern averaging, virtual imaging, and orientation indexing. It also mitigates bias from beam instability or sample heterogeneity. Most importantly, this strategy lays the foundation for real-time, automated experimentation in 4D-STEM by enabling consistent, model-friendly data streams—an essential requirement for closed-loop feedback systems that couple data acquisition with on-the-fly analysis[40].

Ellipse Calibration

The performance of the proposed ellipse calibration framework was evaluated on both crystal and amorphous diffraction patterns, as shown in Figure 4. In the crystal case, uncalibrated patterns exhibit pronounced ellipticity in the diffraction rings due to lens aberrations and scanning system non-linearities, while calibration restores the concentric circular symmetry essential for quantitative analyses such as strain measurement. In amorphous diffraction patterns, elliptical distortions result in asymmetric diffuse rings, which are symmetrically restored after calibration, confirming the method's applicability to both ordered and disordered materials.

To quantitatively evaluate the effectiveness of elliptical distortion calibration, radial intensity profiles were computed before and after correction. To better visualize the intensity distribution beyond the central beam, the data were clipped at the 99th percentile, thereby emphasizing the behavior of higher-order diffraction features. In crystal samples, elliptical distortion correction resulted in a pronounced narrowing of the radial intensity peaks, indicative of improved circularity and ring alignment. In amorphous patterns, the elliptical distortion manifests as subtle anisotropy in the diffuse halo, making it difficult to visually assess correction effectiveness through radial intensity profiles alone. The inherently broad and smooth nature of the amorphous rings renders them less sensitive to small elliptic deformations in traditional radial metrics.

To more sensitively quantify the effect of calibration—particularly for disordered structures—we computed the radial standard deviation in polar coordinates. This metric captures intensity fluctuations along each radius and is therefore more

responsive to minor distortions. A substantial reduction was observed for both crystal and amorphous patterns after correction, indicating that radial fluctuations were effectively suppressed. These results confirm that 4D-PreNet restores circular symmetry and enhances structural uniformity across diverse diffraction types, including both periodic and disordered systems.

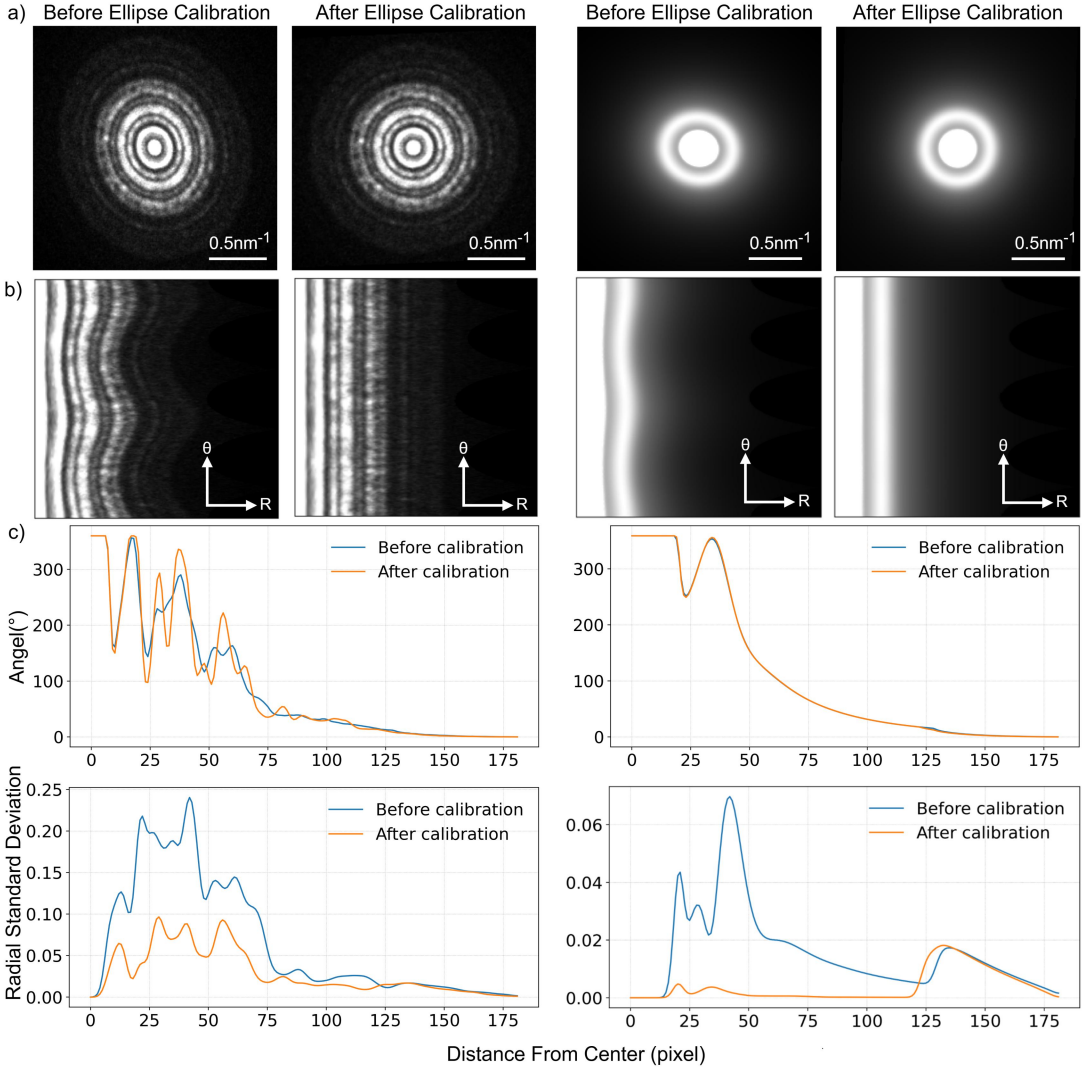

Figure 4: Ellipse calibration of crystal and amorphous samples. (a) Diffraction patterns of both samples before and after ellipse calibration, showing improved ring circularity. (b) Polar coordinate transforms before and after calibration, where uncorrected elliptical distortions appear as sinusoidal patterns, while corrected transforms straighten the rings. (c) Radial integrals (top row) and radial standard deviation (bottom row) as a function of radial distance. calculated from the uncalibrated (blue) and calibrated (orange) patterns.

These results demonstrate that the proposed neural network-based ellipse calibration method can robustly and accurately correct diffraction patterns with significant elliptical distortions. By restoring the true circular symmetry of diffraction rings in both crystal and amorphous materials, the method facilitates reliable extraction of quantitative information, supports downstream analyses such as strain mapping or

radial distribution function calculation, and enables high-throughput, automated 4D-STEM data processing workflows without manual parameter tuning.

4D-PreNet Application on Experiment data

The experimental 4D-STEM dataset acquired from a silicon (Si) sample features a rich variety of structural motifs, including crystal domains, amorphous phases, and regions of mixed order. To evaluate the practical applicability of our framework, we applied 4D-PreNet directly to the raw experimental data cube without additional parameter tuning or manual intervention. As illustrated in Figure 5, the pipeline performs consistently across all structural types.

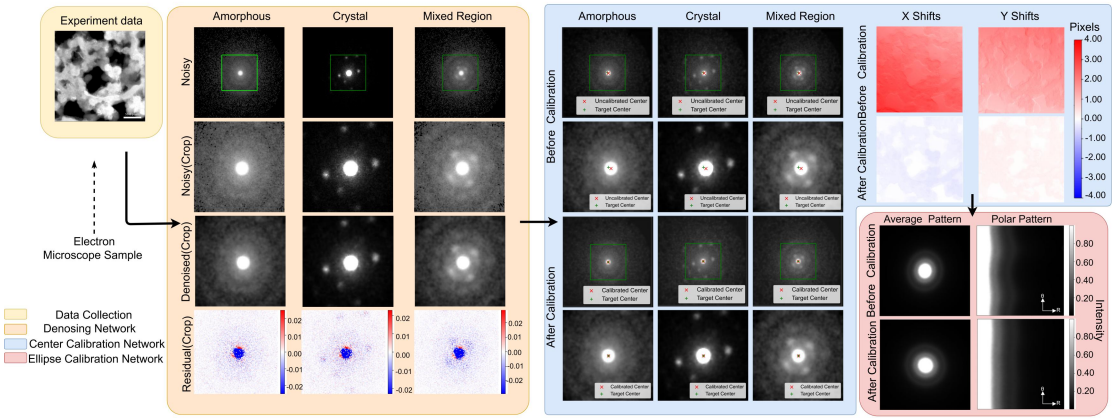

Figure 5: End-to-end preprocessing of experimental 4D-STEM data using 4D-PreNet. Experimental diffraction data were acquired from a silicon (Si) sample containing crystal, amorphous, and mixed-phase regions. The proposed 4DPre-Net framework processes these raw patterns in an end-to-end manner through three sequential modules: denoising, center calibration, and ellipse correction. Left panel (orange): The denoising network effectively suppresses both signal-dependent Poisson noise and additive Gaussian noise, yielding cleaner patterns while preserving structural detail. Residual maps reveal minimal distortion post-denoising. Middle panel (blue): The center calibration module aligns each pattern to the geometric center with sub-pixel precision, as evidenced by the visual overlap between predicted and reference centers. Comparison of X/Y shift maps before and after beam center calibration. The calibrated maps show that global offsets have been effectively removed, confirming accurate alignment of the beam across the entire dataset. Right panel (pink): Elliptical distortion correction restores radial symmetry in the averaged and polar-transformed patterns. Post-calibration patterns exhibit improved circularity and smoother radial decay, indicating suppressed angular variation

In the denoising stage, our model effectively suppresses both signal-dependent Poisson noise and additive Gaussian noise, yielding clean diffraction patterns with enhanced contrast and clarity. In the center calibration stage, the network achieves sub-pixel accuracy, aligning diffraction patterns precisely to the image center regardless of structural disorder. Furthermore, the ellipse calibration model, trained exclusively on synthetic data, generalizes well to real experimental measurements,

correcting anisotropic distortions and restoring circular symmetry in both crystal and amorphous regions.

Importantly, the entire pipeline operates in a fully automated, end-to-end fashion. When executed on a standard NVIDIA GeForce RTX 4090 GPU with a batch size of 128, the complete preprocessing of a full-size (256,256,256,256) 4D-STEM data cube can be completed within 7 minutes. This demonstrates the framework's potential as a fast and scalable solution for real-time, high-throughput 4D-STEM data processing, accelerating automated experimentation and downstream analysis.

Conclusion

We present 4D-PreNet, a fully automated deep learning pipeline developed for preprocessing four-dimensional scanning transmission electron microscopy (4D-STEM) datasets. The framework integrates three essential tasks—denoising, beam center calibration, and elliptical distortion correction—into a unified architecture. Quantitative and qualitative evaluations demonstrate that 4D-PreNet achieves robust and accurate performance across a wide range of material systems, including crystal, amorphous, and mixed-phase regions, and generalizes effectively to previously unseen experimental data. By achieving sub-pixel beam alignment and restoring circular symmetry without manual intervention, the framework enables consistent and reproducible preprocessing suitable for downstream structural analysis. However, the current elliptical distortion correction module assumes the presence of clean, well-defined diffraction rings in the averaged diffraction patterns, which may limit its applicability in structurally complex systems exhibiting overlapping or irregular features. Moreover, under extreme noise conditions where diffraction signals are substantially degraded, the performance of the denoising module may deteriorate. These limitations underscore the need for future improvements to enhance the robustness and versatility of the framework. Despite these challenges, 4D-PreNet marks a meaningful step toward scalable, real-time 4D-STEM data processing. By enabling fast, parameter-free preprocessing of large-scale datasets, it lays the groundwork for future developments in autonomous data acquisition and closed-loop experimental control, contributing to the broader vision of intelligent electron microscopy.

Data availability

The datasets generated and analyzed during the current study are available from the corresponding author upon reasonable request. A representative subset of the simulated and experimental 4D-STEM datasets used for model training and evaluation will be made publicly available upon publication.

Code availability

The code for implementing the 4D-STEM preprocessing framework—including denoising, beam center calibration, and elliptical distortion correction networks—is currently under preparation. It will be released via a public GitHub repository upon

publication to support reproducibility and community use.

Acknowledgement

National Nature Science Foundation of China (52127801) are acknowledged for funding this research. Global Institute of Future Technology at Shanghai Jiao Tong University is also gratefully acknowledged.

Reference

1. Roccapriore KM, Dyck O, Oxley MP, Ziatdinov M, Kalinin SV. Automated Experiment in 4D-STEM: Exploring Emergent Physics and Structural Behaviors. *ACS Nano* 2022, **16**(5)**:** 7605-7614.

2. Kalinin SV, Ophus C, Voyles PM, Erni R, Kepaptsoglou D, Grillo V*, et al.* Machine learning in scanning transmission electron microscopy. *Nature Reviews Methods Primers* 2022, **2**(1)**:** 11.

3. Ophus C. A fast image simulation algorithm for scanning transmission electron microscopy. *Advanced Structural and Chemical Imaging* 2017, **3**(1)**:** 13.

4. Zeltmann SE, Müller A, Bustillo KC, Savitzky B, Hughes L, Minor AM*, et al.* Patterned probes for high precision 4D-STEM bragg measurements. *Ultramicroscopy* 2020, **209:** 112890.

5. Zhang C, Han R, Zhang AR, Voyles PM. Denoising atomic resolution 4D scanning transmission electron microscopy data with tensor singular value decomposition. *Ultramicroscopy* 2020, **219:** 113123.

6. Wu CH, Reynolds WT, Murayama M. A software tool for automatic analysis of selected area diffraction patterns within Digital Micrograph™. *Ultramicroscopy* 2012, **112**(1)**:** 10-14.

7. Lábár JL, Das PP. Pattern Center and Distortion Determined from Faint, Diffuse Electron Diffraction Rings from Amorphous Materials. *Microscopy and Microanalysis* 2017, **23**(3)**:** 647-660.

8. Pekin TC, Gammer C, Ciston J, Minor AM, Ophus C. Optimizing disk registration algorithms for nanobeam electron diffraction strain mapping. *Ultramicroscopy* 2017, **176:** 170-176.

9. Mahr C, Müller-Caspary K, Ritz R, Simson M, Grieb T, Schowalter M*, et al.*

Influence of distortions of recorded diffraction patterns on strain analysis by nano-beam electron diffraction. *Ultramicroscopy* 2019, **196:** 74-82.

10. Yuan R, Zhang J, Zuo J-M. Lattice strain mapping using circular Hough transform for electron diffraction disk detection. *Ultramicroscopy* 2019, **207:** 112837.

11. Savitzky BH, Zeltmann SE, Hughes LA, Brown HG, Zhao S, Pelz PM*, et al.* py4DSTEM: A Software Package for Four-Dimensional Scanning Transmission Electron Microscopy Data Analysis. *Microscopy and Microanalysis* 2021, **27**(4)**:** 712-743.

12. Ziletti A, Kumar D, Scheffler M, Ghiringhelli LM. Insightful classification of crystal structures using deep learning. *Nature Communications* 2018, **9**(1)**:** 2775.

13. Genc A, Kovarik L, Fraser HL. A deep learning approach for semantic segmentation of unbalanced data in electron tomography of catalytic materials. *Scientific Reports* 2022, **12**(1)**:** 16267.

14. Yao L, Ou Z, Luo B, Xu C, Chen Q. Machine Learning to Reveal Nanoparticle Dynamics from Liquid-Phase TEM Videos. *ACS Central Science* 2020, **6**(8)**:** 1421-1430.

15. Aguiar JA, Gong ML, Tasdizen T. Crystallographic prediction from diffraction and chemistry data for higher throughput classification using machine learning. *Computational Materials Science* 2020, **173:** 109409.

16. Han Y, Jang J, Cha E, Lee J, Chung H, Jeong M*, et al.* Deep learning STEM-EDX tomography of nanocrystals. *Nature Machine Intelligence* 2021, **3**(3)**:** 267-274.

17. Mohan S, Manzorro R, Vincent JL, Tang B, Sheth DY, Simoncelli EP*, et al.* Deep Denoising for Scientific Discovery: A Case Study in Electron Microscopy. *IEEE Transactions on Computational Imaging* 2022, **8:** 585-597.

18. Ge M, Su F, Zhao Z, Su D. Deep learning analysis on microscopic imaging in materials science. *Materials Today Nano* 2020, **11:** 100087.

19. Zheng H, Lu X, He K. In situ transmission electron microscopy and artificial intelligence enabled data analytics for energy materials. *Journal of Energy Chemistry* 2022, **68:** 454-493.

20. Kaufmann K, Zhu C, Rosengarten AS, Maryanovsky D, Harrington TJ, Marin E*, et al.* Crystal symmetry determination in electron diffraction using machine learning. *Science* 2020, **367**(6477)**:** 564-568.

21. Xu W, LeBeau JM. A deep convolutional neural network to analyze position averaged convergent beam electron diffraction patterns. *Ultramicroscopy* 2018, **188:** 59-69.

22. Gui C, Zhang Z, Li Z, Luo C, Xia J, Wu X*, et al.* Deep learning analysis on transmission electron microscope imaging of atomic defects in two-dimensional materials. *iScience* 2023, **26**(10)**:** 107982.

23. Sadri A, Petersen TC, Terzoudis-Lumsden EWC, Esser BD, Etheridge J, Findlay SD. Unsupervised deep denoising for four-dimensional scanning transmission electron microscopy. *npj Computational Materials* 2024, **10**(1)**:** 243.

24. Nordahl G, Dagenborg S, Sørhaug J, Nord M. Exploring deep learning models for 4D-STEM-DPC data processing. *Ultramicroscopy* 2024, **267:** 114058.

25. Ge M, Pan Y, Liu X, Zhao Z, Su D. Automatic center identification of electron diffraction with multi-scale transformer networks. *Ultramicroscopy* 2024, **259:** 113926.

26. Ronneberger O, Fischer P, Brox T. U-Net: Convolutional Networks for Biomedical Image Segmentation. In: Navab N, Hornegger J, Wells WM, Frangi AF, editors. Medical Image Computing and Computer-Assisted Intervention – MICCAI 2015; 2015 2015//; Cham: Springer International Publishing; 2015. p. 234-241.

27. He K, Zhang X, Ren S, Sun J. Deep Residual Learning for Image Recognition. 2016 IEEE Conference on Computer Vision and Pattern Recognition (CVPR); 2016 27-30 June 2016; 2016. p. 770-778.

28. Woo S, Park J, Lee J-Y, Kweon IS. CBAM: Convolutional Block Attention Module. *Computer Vision – ECCV 2018: 15th European Conference, Munich, Germany, September 8–14, 2018, Proceedings, Part VII*. Munich, Germany: Springer-Verlag; 2018. pp. 3–19.

29. Han S, Mao H, Dally WJ. Deep Compression: Compressing Deep Neural Network with Pruning, Trained Quantization and Huffman Coding. *arXiv: Computer Vision*

and Pattern Recognition 2015.

30. Lehtinen J, Munkberg J, Hasselgren J, Laine S, Karras T, Aittala M*, et al.* Noise2Noise: Learning Image Restoration without Clean Data. 2018.

31. Ede JM. Deep learning in electron microscopy. *Machine Learning: Science and Technology* 2021, **2**(1)**:** 011004.

32. Bengio Y. Practical Recommendations for Gradient-Based Training of Deep Architectures. In: Montavon G, Orr GB, Müller K-R (eds). *Neural Networks: Tricks of the Trade: Second Edition*. Springer Berlin Heidelberg: Berlin, Heidelberg, 2012, pp 437-478.

33. Sun K, Xiao B, Liu D, Wang J. Deep High-Resolution Representation Learning for Human Pose Estimation. 2019 IEEE/CVF Conference on Computer Vision and Pattern Recognition (CVPR); 2019 15-20 June 2019; 2019. p. 5686-5696.

34. Zhang C, Bengio S, Hardt M, Recht B, Vinyals O. Understanding deep learning (still) requires rethinking generalization. *Commun ACM* 2021, **64**(3)**:** 107–115.

35. Ruiz N, Chong E, Rehg J. *Fine-Grained Head Pose Estimation Without Keypoints*, 2018.

36. Tuan Rashid TMN, Mohd Fadzil L, Omar M. 3D Bounding Box Estimation Using Deep Learning and Geometry Based on Yolov7 Output on Single-Board Computer. *International Journal of Electrical and Electronics Engineering* 2024, **11:** 77-84.

37. Jain A, Ong S, Hautier G, Chen W, Richards W, Dacek S*, et al.* Commentary: The Materials Project: A materials genome approach to accelerating materials innovation. *APL Materials* 2013, **1:** 011002.

38. Shorten C, Khoshgoftaar TM. A survey on Image Data Augmentation for Deep Learning. *Journal of Big Data* 2019, **6**(1)**:** 60.

39. Kingma D, Ba J. Adam: A Method for Stochastic Optimization. *International Conference on Learning Representations* 2014.

40. Shi C, Cao MC, Rehn SM, Bae S-H, Kim J, Jones MR*, et al.* Uncovering material

deformations via machine learning combined with four-dimensional scanning transmission electron microscopy. *npj Computational Materials* 2022, **8**(1)**:** 114.